

**Titolo**
**Studi preliminari di tecniche di monitoraggio del nocciolo di ALFRED**
**Descrittori**

**Tipologia del documento:** Rapporto Tecnico  
**Collocazione contrattuale:** Accordo di programma ENEA-MSE su sicurezza nucleare e reattori di IV generazione  
**Argomenti trattati:** Reattori veloci  
 Generation IV Reactors

**Sommario**

Ad ulteriore avanzamento del progetto di nocciolo del reattore dimostrativo ALFRED, così come concepito in seno al progetto di ricerca LEADER del 7° Programma Quadro EURATOM, nel presente rapporto si presentano e discutono i risultati preliminari di due studi, entrambi relativi ad aspetti di monitoraggio del nocciolo, e precisamente:

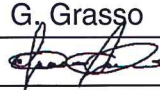
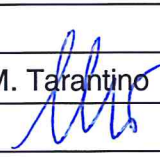
- una valutazione teorica dell'efficacia di una rete di rivelatori neutronici posti all'esterno della zona attiva del nocciolo, con particolare attenzione alla loro capacità di individuare modifiche nella distribuzione spaziale del flusso nel nocciolo;
- una definizione preliminare di un sistema alternativo di individuazione della posizione da cui si verifichino eventuali dispersioni di prodotti di fissione nel circuito primario per rottura della guaina delle barrette di combustibile, operante per analisi della radioattività raccolta nel cielo di pila.

**Note**

**Autori:** A. Guglielmelli<sup>1</sup>, G. Grasso<sup>2</sup>, F. Lodi<sup>1</sup>, R. Lo Frano<sup>3</sup>, D. Mattioli<sup>2</sup>,  
 C. Petrovich<sup>2</sup>, M. Sumini<sup>1</sup>

- (1) Università di Bologna  
 (2) ENEA  
 (3) Università di Pisa

**Copia n.**
**In carico a:**

2			NOME			
			FIRMA			
1			NOME			
			FIRMA			
0	EMISSIONE	25/09/14	NOME	G. Grasso	M. Tarantino	M. Tarantino
			FIRMA			
REV.	DESCRIZIONE	DATA		REDAZIONE	CONVALIDA	APPROVAZIONE

## Table of Contents

1.	Introduction .....	3
2.	Spatial Flux Measurements .....	3
2.1.	State of the Art Review .....	3
2.2.	Guidelines Parameters to Detect .....	4
2.3.	Positioning and Efficiency .....	6
3.	Cladding Failure Detection System.....	11
3.1.	General methodology .....	11
3.1.1.	Selection of tag gases .....	11
3.1.2.	"Cocktail" preparation principles .....	12
3.1.3.	Quanta definition.....	12
3.1.4.	Uncertainties propagation.....	14
3.1.5.	Fingerprints .....	17
3.1.6.	Families .....	18
3.2.	Application to the ALFRED design .....	19
4.	Conclusions .....	24
	References .....	25

 <b>Ricerca Sistema Elettrico</b>	<b>Sigla di identificazione</b>	<b>Rev.</b>	<b>Distrib.</b>	<b>Pag.</b>	<b>di</b>
	ADPFISS – LP2 – 051	0	L	3	25

## 1. Introduction

The monitoring of the core status is of paramount importance for a nuclear reactor, in order to retrieve exhaustive information notably on the neutron flux level and on its spatial distribution, the reactivity of the system, the distribution of coolant temperatures at core outlet and the integrity of the cladding (being the first engineering barrier against the diffusion of radioactivity in the system). Once all this information is available, both the operational control of the reactor and the actuation of the reactor protection system are made possible.

This general statement assumes even more relevancy when addressed to a demonstration reactor such as ALFRED (the Advanced Lead-cooled Fast Reactor European Demonstrator), for which redundant, reliable and precise monitoring of the core is a mandatory design constraint.

While for the monitoring of coolant temperatures wide experience is already available in the European Heavy Liquid Metal (HLM) community, thanks to the operation of several lead and lead-bismuth eutectic (LBE) loops and pools, very few information can be retrieved for the neutron detection in a HLM environment, as well as on the detection of fission gases in the primary system.

The work here reported aims at addressing these issues, by performing preliminary studies on a system of neutron detectors positioned ex-core and at assessing their effectiveness in monitoring the flux level and spatial distribution. Moreover, the conceptual design of a tagging technique for the fuel elements, allowing the unique identification of breached claddings, will be proposed.

## 2. Spatial Flux Measurements

In the ALFRED core design considered in the present work – the one resulting from the LEADER EURATOM FP7 project [1] and exhaustively reviewed in a companion deliverable [2] –, no instrumentation has been initially foreseen, nor in-core positions allocated, mostly because of the conceptual stage of the project. Aiming at advancing the status of the project towards a more mature level, a preliminary investigation has been performed to verify the viability of ex-core detectors to what concerns the monitoring of the flux level and its spatial distribution in the core.

### *2.1. Guidelines and Parameters to Detect*

As mentioned above, neutron detectors must provide information on the status of the reactor for both its regular control and its protection against initiating events.

For reactor control, the overall flux level (notably during startup) and its spatial distribution (with particular attention to the one close to full power operation) have to be carefully monitored. Concerning reactor protection, fast differential flux monitors are deemed necessary to monitor the criticality changes so as to trigger the timely intervention of the Reactor Protection System (RPS) before reaching any situation potentially leading to unmanageable conditions.

According to these general guidelines, some considerations can be drawn:

 <b>Ricerca Sistema Elettrico</b>	<b>Sigla di identificazione</b>	<b>Rev.</b>	<b>Distrib.</b>	<b>Pag.</b>	<b>di</b>
	ADPFISS – LP2 – 051	0	L	4	25

- a first means for the control of the flux level – either slow and fast, that is: reactivity – can be the use of detectors placed far from the reactor core (e.g.: ex-vessel), as typically done in fast reactors;
- a second, redundant monitoring of the flux level is deemed necessary to provide a further means of monitoring which is reckoned important in a demonstrator reactor such as ALFRED;
- the monitoring of the spatial distribution of the neutron flux is to be achieved by means of detectors placed as close as possible to the reactor core, in order to maintain information on the flux shape (that is, at a distance corresponding to the lowest number of mean free paths that can be achieved complying with fuel assembly design).

Due to the need for close-to-core detectors for spatial flux distribution monitoring, the second, redundant monitoring of the flux level might be provided as well by this detection system. Accordingly, in the following the two systems will be identified as:

1. Full-Range Flux Detection (FRFD) system, for the ex-vessel set of neutron detectors with operation range from startup to full power;
2. Operation Monitoring and Protection Detection (OMPD) system, for the in-vessel ex-core set of neutron detectors devoted only to full-power flux level monitoring and spatial flux mapping.

## ***2.2.State of the Art Review***

Neutron detectors operating in a fast flux have been developed in the past, and successfully implemented in all experimental and power reactors operating all over the World. Anyway, all the latter rely on the technology of sodium-cooling, which might arise the issue of the transferability of these detectors to a different environment.

Apart from the need of protection of the in-vessel probes from the harsh environment itself, which is a matter of chemical compatibility of the casing with the HLM and which – in a final analysis – can be bypassed by enveloping the probe in a protective shield, for all detectors the crucial point is the ability to respond to a signal which is spectrally different: hence, to a response function which is superposed to a flux distribution that might not fit to give a relevant signal.

On the other hand, it is worth noting that the self-shielding properties of lead against  $\gamma$  rays strongly simplify the protection of the detectors, which is required to allow their correct operation (typical limits are up to  $10^4$  Gy/h for fission chambers and up to 10 Gy/h for boron counters).

Concerning the FRFD system, different typologies of detectors are to be implemented out of the main vessel in order to span throughout the entire range of neutron flux, from start up to full power – including the intrinsic neutron source from spontaneous fission of Pu240 and, possibly, of Am242. The typical choice for fast reactors, which can be envisaged also for ALFRED, focuses on:

- boron counters for low-power operation (including start up monitoring and refueling control);

- fission chambers for mid-range operation;
- compensated ion chambers for power-range operation.

Possible shielding of these detectors might be envisaged, by means of moderating and/or absorbing media, for reducing the noise from different sources than the reactor core, while leaving sufficiently high the signal coming from the core itself. On the other hand, no gamma shielding (typically, by lead blocks) is envisaged thanks to the presence of lead within the vessel.

Concerning the OMPD system, no reference was found in literature for driving the selection of detector typologies and positioning, making this system the actual object of the first part of the present report.

A review of the state-of-the-art on neutron detectors for fast reactors application led to the identification of PHOTONIS as possible supplier, thanks to its experience in providing detectors for both Phenix and Superphenix, developed in cooperation with CEA.

According to the list of available products, and – among these – selecting the ones designed to operate in the temperature field envisaged for ALFRED, two fission chambers (with integral cable) are found out. The characteristics of these two detectors are summarized in Table 2.1.

**Table 2.1: Technical specifications of the selected neutron detectors envisaged for ALFRED [3]**

		<b>unit</b>	<b>CFUC 06</b>	<b>CFUE 32</b>
Neutron sensitivity	Current mode	$A/n \text{ cm}^{-2} \text{ s}^{-1}$	$2 \cdot 10^{-13}$	$10^{-16}$
	Fluctuation mode	$A^2 \text{ Hz}^{-1}/n \text{ cm}^{-2} \text{ s}^{-1}$	$4 \cdot 10^{-26}$	$4 \cdot 10^{-29}$
	Pulse mode	$c \text{ s}^{-1}/n \text{ cm}^{-2} \text{ s}^{-1}$	1	$10^{-3}$
Pulse operating range		$n \text{ cm}^{-2} \text{ s}^{-1}$	$1 \div 10^5$	$10^3 \div 10^8$
Max operating T		°C	600	600
Nominal diameter		mm	48	7
Nominal detector length		mm	412	150
Nominal sensible length		mm	230	56

Both detectors are designed to detect thermal neutrons ( $E < 0.025 \text{ eV}$ ), so that the Ar-filled chamber is lined (thickness range being  $0.06 \div 2 \text{ mg/cm}^2$ ) with highly enriched (>90%) U electronically deposited on the cathode, to exploit its high fission cross section. This choice has been driven to enhance the response of these detectors, envisaged for use out of the vessel of LWRs, where the neutron flux is low and thermal. In our specific case, instead, the use of detectors into the vessel for power-range measurements – hence exposed to a sensibly higher neutron flux – might result in an excessive response, going out of the detectability range.

Fortunately, being employed in a fast system, the responses per incident neutron are lowered according to the diminishing cross section of U235 (red curve in Figure 2.1), which might result in a sufficiently reduced sensibility of the fission chambers to open the possibility of placing detection systems within the main vessel and, possibly, close to the core, as aimed. Whether the sensibility of U235-lined detectors should still overcome the expected responses close to the core, the alternative use of U238 can be considered (green curve in Figure 2.1).

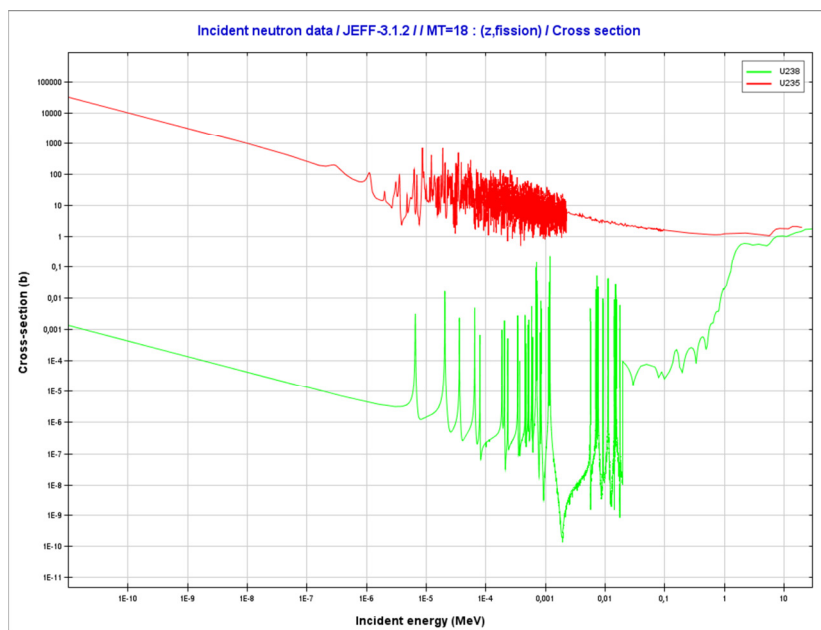


Figure 2.1 - Plot of U235 (red) and U238 (green) fission cross sections. Data from JEFF3.1.2 [4] nuclear data library.

### 2.3. Positioning and Efficiency

In Figure 2.2 a scheme of the ALFRED core is given, showing the apportionment of the multiplying region into an inner core (with lower enrichment fuel, yellow positions) and an outer core (red positions) for power flattening purposes; the positioning of Control Rods (CRs in blue and SRs in green positions, respectively); and the dummy elements shielding the inner vessel (white positions).

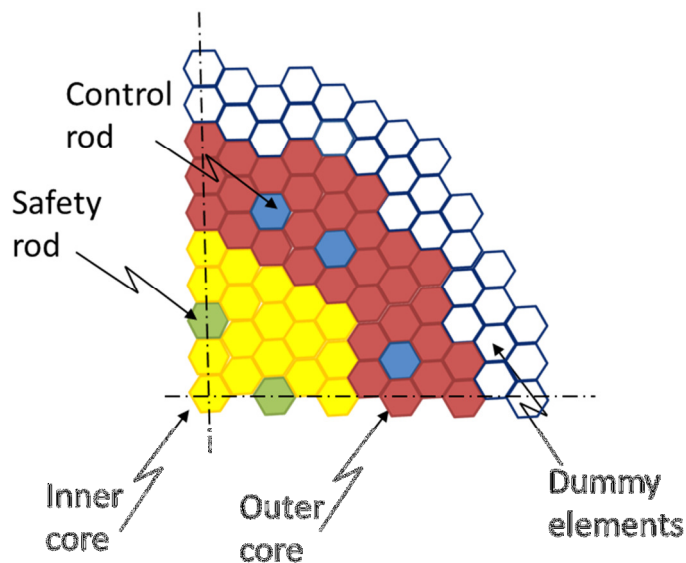


Figure 2.2 - Scheme of the ALFRED core (one quarter).

The flattening of the power/FA distribution was assumed as a pillar for the neutronic characterization of the core, in order to enhance the average power density as much as

possible (for fuel economy) while maintaining the peak power density (notably: the maximum linear power) below the reference value. This allows the respect of the safety margins for the fuel temperature (for a more comprehensive description of the design approach, and further details on the results of the neutronic characterization, see [5]). This is why its monitoring is one of the main goals of the OMPD system.

The second main goal of the OMPD system is to promptly detect any possible initiator eventually leading either to strong deformations in the power/FA distribution or positive changes in the reactivity of the system, so as to actuate a response through the triggering of the RPS intervention before any excess of power density or over-criticality might pose concerns. One of the most challenging events, leading to both the effects abovementioned, is the spurious inadvertent withdrawal of one CR, which are therefore to be carefully looked for in defining the positioning of the OMPD system.

According to the mechanical design of the fuel elements, the steel “nose” foreseen at the end of the hexagonal wrapper (the red element in the left frame of Figure 2.3) to facilitate the exit of the coolant towards the hot collector and then the steam generators, is exploited. Within such nose, indeed, a cavity machined from the top was envisaged for housing probes and detectors, driven as close as possible to the active zone. The vertical cross section of a FA shown in the same frame of Figure 2.3 also allows to visualize the relative position of the fuel bundle (only one fuel pin is shown for better clearness), and the top of the active zone within it (the black region represents the stack of fuel pellets).

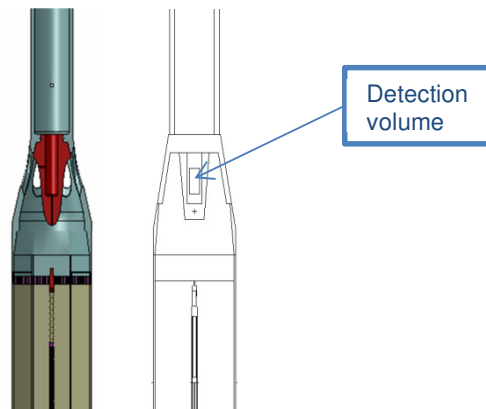


**Figure 2.3 - Scheme of the ALFRED FA (end of fuel bundle, core outlet and funnel, from bottom to top) (left). The position envisaged for hosting the instrumentation is the red nose at core outlet. MCNP model of the same region (right) with indicated the detection volume within the steel nose.**

In order to correctly simulate the response of the neutron detectors, a very detailed heterogeneous core model has been set up in MCNP6 [6], including the outlet nose and its internal volume, as shown in the geometry plot of Figure 2.3 (right frame).

Finally, the positioning of the detectors on the core map has been made by choosing some elements, out of the 171 available, according to the following selection criteria:

- every fuel element should be provided of a neutron detector, or be adjacent to an instrumented one;
- around every CR at least three fuel elements should be provided of neutron detector (so as to ensure the 2 out of 3 response logic).

It is worth saying that another set of neutron detectors (not considered in the present study) is envisaged in the dummy elements of the innermost ring of the neutron reflector: these detectors also belong to the OMPD system, and are aimed at providing information on the axial flux distribution.

The result of the selection of the fuel elements to be instrumented for the OMPD system is shown on the whole core map of Figure 2.4 by light gray circles. Figure 2.4 also shows the numbering of the FAs (the last two digits, i.e.  $\_XX$ ) that will be used in the rest of this chapter for presenting the results; the hundreds (either 2\_\_ or 3\_\_) indicate instrumented and not instrumented FAs, respectively. It should be noted that, while the FA positions fully exploit the  $\frac{1}{4}$  symmetry of the core, the detectors are not fully symmetrical in the innermost region mainly because of the excessive redundancy possibly resulting otherwise.

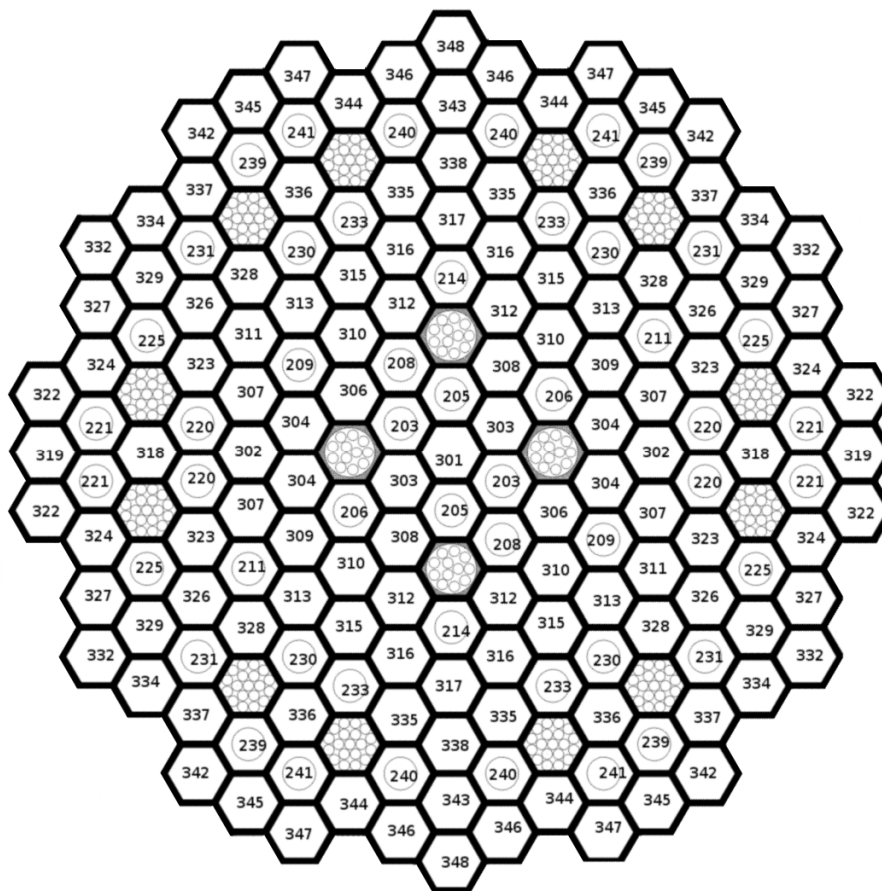


**Figure 2.4 - Numbers identifying the FA positions on the ALFRED core map. The hundreds (either 2xx or 3xx) indicate instrumented and not instrumented FAs, respectively.**

As a starting point for evaluating the effectiveness of the proposed neutron detection system, a typical operating condition, with all CRs partially and evenly inserted into the active region, is simulated, to check whether the OMPD system is able to reproduce the power/FA distribution.

A demanding MCNP6 [6] simulation has been run to decrease the Monte Carlo standard deviations to values not higher than 7%. Neutron cross section data have been taken from the JEFF3.1.2 [4] library. The results of the simulation – notably FA power and detector response – are presented in Figure 2.5.

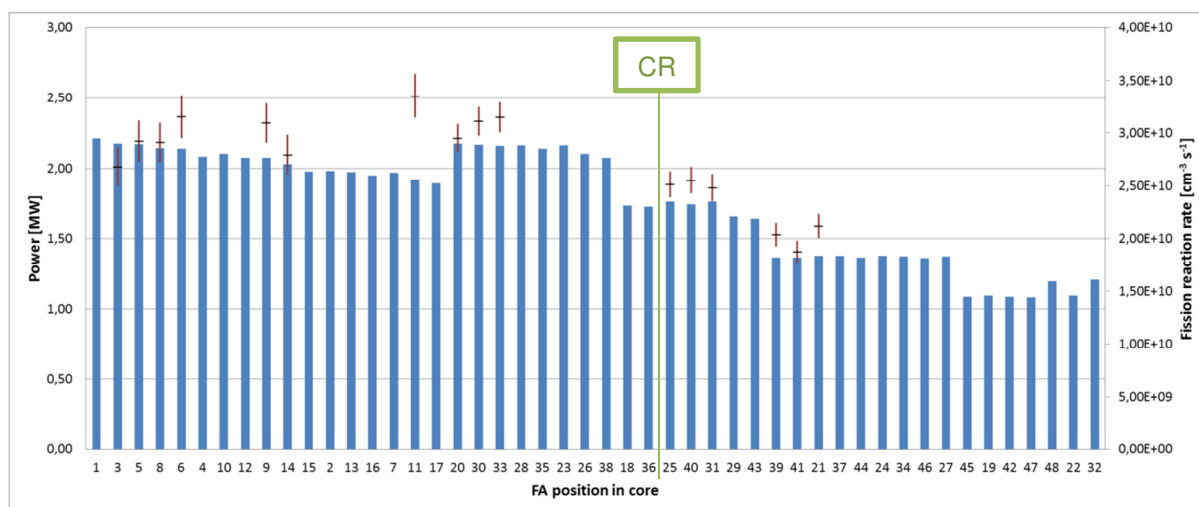


**Figure 2.5 - Power/FA and detector response at BoL with all CRs partially inserted in the core. The results are plotted according to the distance from core centre (FA numbering as explained in Figure 2.4).**

To have a quantitative perception of the quality of the results, in terms of agreement between the spatial behavior of the detector response and the one of the power of the corresponding FA, in Figure 2.6 the actual ratio of the detector response and the corresponding FA power is plotted only for the instrumented FAs, normalized on a reference ratio computed between the average detectors response and the average power of the corresponding FAs. From the graph it is possible to see that – apart from few points – all results lie well into the 10% error band, the standard deviation of the majority of the points even including the reference line. It is also worth noting that the detectors close to the core center suffer from the proximity of the SRs, whose absorbing part – in withdrawn position – gets aside the detectors themselves.

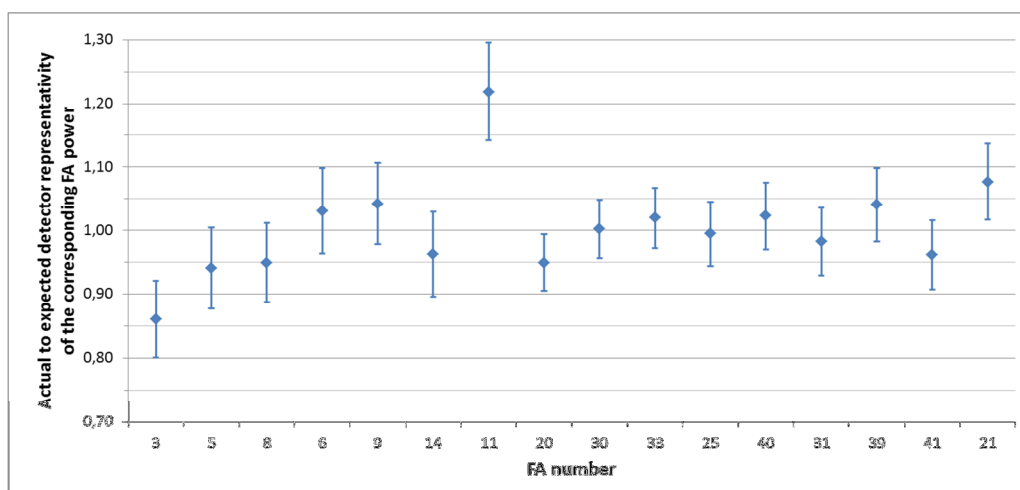


**Figure 2.6 - Power/FA and detector response at BoL with all CRs partially inserted in the core. The results are plotted according to the distance from core centre (FA numbering as explained in Figure 2.4).**

Another key result it is worth mentioning is that the detector response – supposing the fissile material employed is U238 instead of U235, and according to the different effective reaction rates of these two isotopes in the neutron spectrum of interest (see Figure 2.1) – seems to comply with the current operating range of type “CFUE 32” detectors. Indeed, the neutron sensitivity of this detector (Table 2.1) is  $10^{-16}$  A/n  $\text{cm}^{-2} \text{s}^{-1}$ , and the associated electronics embed a pico-ampere meter. Considering that the reference sensitivity has been provided

assuming the sensitive layer is made of U235, hence scaling the latter to the ratio of the effective cross sections of U238 and U235 ( $\sim 10^{-3}$ ), under the neutron flux at the positions envisaged for the OMPD system ( $\sim 10^{13}$  n cm<sup>-2</sup> s<sup>-1</sup>) a signal in the order of the  $\mu$ A should be expected, which might fit with the electronics of the PHOTONIS device.

The second, relevant test regards the simulation of a perturbed condition in which one of the CRs is extracted from the active region, all others remaining in position. Actually, all the results have been summed up by exploiting the ¼ core symmetry, in order to minimize the statistical errors: accordingly, four symmetrical CRs have been withdrawn from the core to better simulate the effect of one single rod exiting the active region.

As can be seen by the plot in Figure 2.7 and by comparison with the reference plot in Figure 2.5, the response of the detectors adjacent to the withdrawn CRs (positions “20”, “21” and “25”) is increased coherently with the increased power of the corresponding FAs. The indication of the maintained proportionality between the two observables despite their increase is shown in Figure 2.8, where the  $\pm 10\%$  trend lines are plotted for reference.

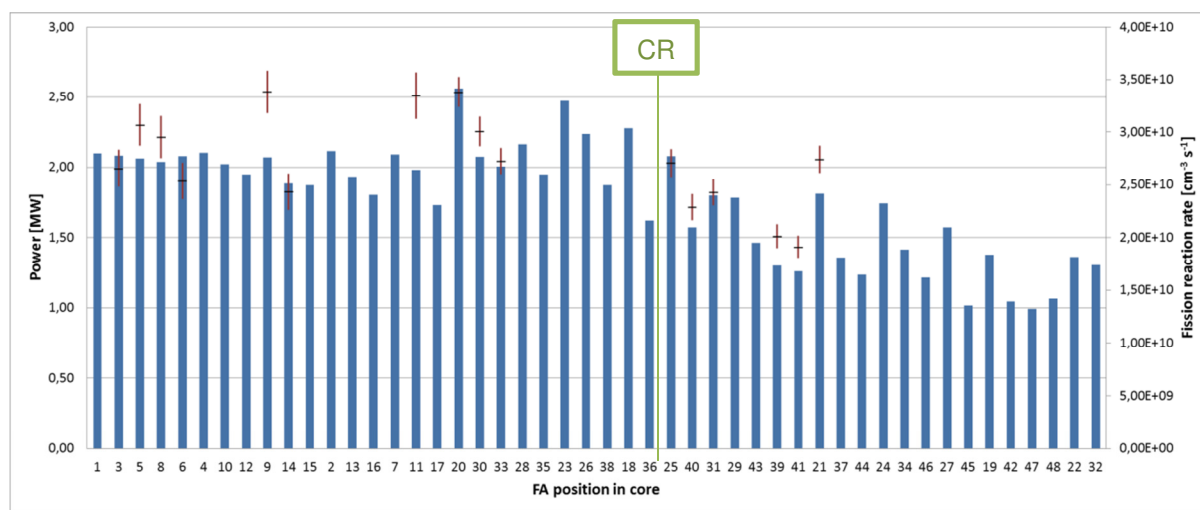


**Figure 2.7 - Power/FA and detector response at BoL with all CRs partially inserted in the core but four, symmetrical. The results are plotted according to the distance from core centre (FA numbering as explained in Figure 2.4).**

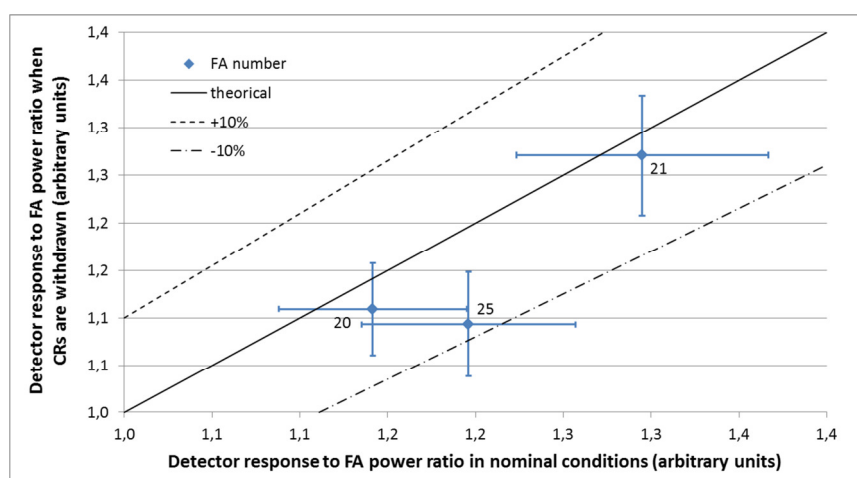


**Figure 2.8 - Ratio between the detector response and the power/FA at BoL for the three elements adjacent to the CR being withdrawn (FA numbering as explained in Figure 2.4).**

 <b>Ricerca Sistema Elettrico</b>	<b>Sigla di identificazione</b>	<b>Rev.</b>	<b>Distrib.</b>	<b>Pag.</b>	<b>di</b>
	ADPFISS – LP2 – 051	0	L	11	25

### 3. Cladding Failure Detection System

A sound and elegant methodology, originally developed by C. Artioli [7] for the PRISM reactor, for detecting and identifying a breached assembly is presented in some detail in the present report along with its adaption and application to the ALFRED core. Indeed, precisely locating the occurrence of a failure has a huge safety and economic impact on the robustness of a reactor design; for these reasons it is mandatory to develop a simple and sound system able to perform such function, with some reliability, without interfering with the normal operation of the reactor.

#### 3.1. General methodology

The founding principle of the identification system is to attach some kind of blueprint to each fuel assembly (FA) by inserting a “cocktail” of tag gases into every pin and to detect their loss by means of their daughters’ activity. The tag gas mix and their mutual ratios will be different and unique for each FA, so that the spectrometric analysis of the energy and number of the daughters’ emitted gamma can unambiguously identify the faulted assembly. An easy question could arise by now: why select parent that via neutron capture yield unstable isotopes while we can directly use the daughters which are the real one that will be detect? as much is easy the answer, in order to take advantage of the continuous production term by the parent which will make possible to minimize the initial load of gas and thus relieving EoL clad stresses.

##### 3.1.1. Selection of tag gases

Tag gases must abide a number of requirements in order to be a practical solution for a long term identification system, such as the followings:

- parents and daughters must be different from any cover gas or fission product,
- parents and daughters have not to be chemically reactive with any reactor components (i.e. they have to be noble gases),
- parent activation cross section must balance the opposite requirements of being low enough to consider the isotope stable or almost stable compared to the FA life and, at the same time, being high enough in order to produce a significant quantity of daughter,
- daughter decay constant has to be low enough to allow a significant equilibrium concentration, but high enough to present a detectable activity.

With these guidelines four gases have been selected, listed in Table 3.1, which are basically the only viable options for a MOX fueled fast reactor.

**Table 3.1: Selected parent-daughter pairs**

Parents			Daughters		
Isotope	Fast $\sigma$ [b]	Fast irradiation half-life ( $\Phi = 10^{15}$ n/cm <sup>2</sup> s) [y]	Isotope	Half-life	Number of $\gamma$ s
Kr78	0.007	3100	Kr79	1.455 d	3
Xe124	4.0	5.5	Xe125	17 h	2
Xe126	0.05	440	Xe127	36.41 d	2
Xe128	0.01	2200	Xe129m	8.89 d	1

The irradiation half-life of the parent gases is long in relation to the FA in-core life except for Xe124, this assures an acceptable depletion rate during the FA life. The short half-life of the daughters allows the equilibrium concentration to be reached in weeks or months (for the Xe127), therefore a good accuracy in the calculation of ratios is reachable as will be demonstrated later.

### 3.1.2. "Cocktail" preparation principles

It must be kept in mind that the final objective is to calculate any initial tag gas quantity from daughters' activity and for that an accurate knowledge of the activation and decay history of the FA is required. To handle this issue two ways are possible:

1. working with absolute quantities or
2. using ratios,

so different to one another in order to accommodate all the uncertainties involved (more in the next sub-section). Ratios are much more stable and less sensitive to error than absolute quantities so seems convenient to work with them; for this reason they will be our target in the present methodology.

It is common for medium to large reactor to have hundreds of FAs loaded in the core so it is apparent that all the possible combinations of four gases are not going to be nearly enough; another variable is to be called upon, and – among the available ones – the "quantity" is chosen. Modifying in turn the amount of each gas makes possible to create different ratios and thus different fingerprints to put in each FA. With this strategy it is feasible to create as many different fingerprints as required, but a question must find its answer first: How much two fingerprints have to differ so that they will be, without fail (engineering speaking), distinguished? A thorough discussion will be brought in subsection 3.1.4.

### 3.1.3. Quanta definition

The starting point of the analysis is the definition of the minimum quantities of tag gas to load in order to have a detectable daughter's activity in some limiting situations, so to ensure in

 <b>Ricerca Sistema Elettrico</b>	<b>Sigla di identificazione</b>	<b>Rev.</b>	<b>Distrib.</b>	<b>Pag.</b>	<b>di</b>
	ADPFISS – LP2 – 051	0	L	13	25

every credible scenario that the breach will be effectively detected. We call this minima, *quanta*.

At first the balance equation for parents and daughters has to be set up. The former has only the capture disappearance term

$$N_p(t) = N_{po} e^{-\sigma\Phi t} \quad (3.1)$$

where  $N_p$  is the parent atomic density,  $N_{po}$  is the initial load amount and  $\Phi$  is the flux, while the latter has to include two terms to reproduce the different behaviors during reactor operation: an initial build-up towards equilibrium (reached thanks the short half-life) and then a decreasing according to parent depletion

$$dN_d(t) = (-\lambda N_d(t) + \sigma\Phi N_{po} e^{-\sigma\Phi t}) dt \quad (3.2)$$

where  $N_d(t)$  is the daughter atomic density and  $\lambda$  is the decay constant.

The limiting scenarios which constrain the quanta are: at the FA End of Life (EoL) when the parent concentration is at a minimum and at the last restart before EoL when daughters build up is at a minimum.

#### EoL scenario

Equation (3.2) becomes in this situation

$$dN_d(t) = (-\lambda N_d(t) + \sigma\Phi N_{po} e^{-\sigma\Phi T}) dt \quad (3.3)$$

where T is the equivalent assembly life in the reference flux  $\Phi$ . The solution is

$$\lambda N_d(t) = \sigma\Phi N_{po} e^{-\sigma\Phi T} (1 - e^{-\lambda t}) \quad (3.4)$$

which – if the last restart is far enough (i.e. weeks), thus at equilibrium conditions, simplifies to

$$\lambda N_d(t) = \sigma\Phi N_{po} e^{-\sigma\Phi T} \quad (3.5)$$

The escaped daughter gas, in a clad rupture event, will be dispersed, along with the parent and the other fission products in the cover gas, whose a sample (as much as a fraction  $D$ ) will be collected and analyzed by the detector after a delay time  $\tau$  from escaping. Then the activity at the detector will be

$$A(\tau) = D\lambda N_d(t) e^{-\lambda\tau} = D\sigma\Phi N_{po} e^{-(\sigma\Phi T + \lambda\tau)} \quad (3.6)$$

where  $A(\tau)$  is the measured activity.

Now, if the sensibility of the detector is supposed to be  $S$  [ $\gamma/s$ ], we want

$$A(\tau) > S \quad (3.7)$$

or explicitly

$$D\lambda N_d(\tau) e^{-\lambda\tau} = D\sigma\Phi N_{po} e^{-(\sigma\Phi T + \lambda\tau)} > S \quad (3.8)$$

from which we can calculate the quanta as

 <b>Ricerca Sistema Elettrico</b>	<b>Sigla di identificazione</b>	<b>Rev.</b>	<b>Distrib.</b>	<b>Pag.</b>	<b>di</b>
	ADPFISS – LP2 – 051	0	L	14	25

$$N_{po \min \text{ EoL}} = \frac{S e^{\sigma\Phi T + \lambda\tau}}{D\sigma\Phi} \quad (3.9)$$

### Restart scenario

The other critical scenario is logically the most tight because after restart the daughters' activity is nearly zero and quickly build up with irradiation. If a breach occurs very close to restart it will not be detect and in fact will never be in the FA in question because the tag gases are lost forever. This is a weak point of the present methodology which can be alleviated, but not eliminated; the key brick is the assumed black-out time  $T_{BO}$ , the time in which we consider improbable a breaching event and after which the activity is back at near detectable levels. The shorter the black out time the higher will be the quanta so a balance must be strike-out.

That being said the solution at the end of the accepted black out time (EoBO) is

$$\lambda N_d(t) = \sigma\Phi N_{po} e^{-\sigma\Phi_a C} (1 - e^{-\lambda T_{BO}}) \quad (3.10)$$

where  $C$  is the time from BoL and the last restart,  $\Phi_a$  is the average flux during time  $C$  and in this context  $\Phi$  is the actual flux after restart.

For the same mechanisms already explained in the preceding scenario the activity at the detector is

$$A(\tau) = D\sigma\Phi N_{po} e^{-(\sigma\Phi_a C + \lambda\tau)} (1 - e^{-\lambda T_{BO}}) \quad (3.11)$$

and thus the quanta for the restart scenario is

$$N_{po \min \text{ EoBO}} = \frac{S e^{\sigma\Phi_a C + \lambda\tau}}{D\sigma\Phi (1 - e^{-\lambda T_{BO}})} \quad (3.12)$$

The most restrictive scenario is usually EoBO although it depends strongly on the black out time assumed. It is worth stressing that now two set of quanta are to be handled, so that various possibilities open: these will be discussed at the end of the next section, after the uncertainties analysis.

### *3.1.4. Uncertainties propagation*

The various fingerprints can be created by simple increasing the parent density compared to the quanta and It's now time to answer the question: How much I have to make two fingerprints different so that they will be, without fail (engineering speaking), distinguished? Enough to accommodate every uncertainties involved in the regression from the daughter activity to the initial parent loading. So these uncertainties must now be quantified in each limiting scenario.

### EoL scenario

The ratio of the signal of two daughters is expressed as

$$R_{ij} = \frac{A_i}{A_j} = \left( \frac{N_{po i}}{N_{po j}} \right) \left( \frac{\sigma_i}{\sigma_j} \right) (e^{-\Delta\sigma_{ij}\Phi T}) (e^{-\Delta\lambda_{ij}\tau}) \quad (3.13)$$

 <b>Ricerca Sistema Elettrico</b>	<b>Sigla di identificazione</b>	<b>Rev.</b>	<b>Distrib.</b>	<b>Pag.</b>	<b>di</b>
	ADPFISS – LP2 – 051	0	L	15	25

where  $\Delta\sigma_{ij} = \sigma_i - \sigma_j$ , which can be compacted in the form

$$R_{ij} = R_o R_e R_d R_a \quad (3.14)$$

where

$R_o = \frac{N_{p o i}}{N_{p o j}}$  expresses the initial ratio between the  $i$  and  $j$  tag gases,

$R_e = \frac{\sigma_i}{\sigma_j}$  is the ratio between efficiencies in producing daughters  $i$  and  $j$  and their equilibrium activities,

$R_d = e^{-\Delta\sigma_{ij}\Phi T}$  is the difference between parents depletion and

$R_a = e^{-\Delta\lambda_{ij}\tau}$  is the difference between daughters decay before being detected.

Each of these parameters has its own uncertainties that will propagate to  $R_{ij}$  and thus to the initial theoretical ratio. In the following all the  $R$  terms will be considered independent from each other for easiness, although there's correlation between  $R_e$  and  $R_d$  through the cross sections, since they have a compensating effect on each other is conservative to take them independent.

The elementary parameters, that we will propagate, are the initial loading, the cross sections, the flux and the time delay which will be indicated respectively as  $\frac{\delta R_o}{R_o}$ ,  $\frac{\delta\sigma}{\sigma}$ ,  $\frac{\delta\Phi}{\Phi}$  and  $\delta\tau$ .

$R_o$  The error on the first R term is easy done since, by definition, is equal to  $\frac{\delta R_o}{R_o}$

$R_e$  Combining statistically the errors on the  $i$ -th and  $j$ -th cross sections we got

$$\frac{\delta R_e}{R_e} = \sqrt{\left(\frac{\delta\sigma_i}{\sigma_i}\right)^2 + \left(\frac{\delta\sigma_j}{\sigma_j}\right)^2} = \sqrt{2} \frac{\delta\sigma_i}{\sigma_i} \quad (3.15)$$

since the relative error on the cross sections is assumed equal for every isotope

$R_d$

$$\frac{\delta R_d}{R_d} = \delta(\Delta\sigma_{ij}\Phi T) = \frac{\delta\sigma}{\sigma} \Delta\sigma_{ij}\Phi T + \Delta\sigma_{ij}\delta(\Phi T) \quad (3.16)$$

$R_a$

$$\frac{\delta R_a}{R_a} = \delta\tau\Delta\lambda_{ij} . \quad (3.17)$$

The errors can finally be combined statistically to give the uncertainty on  $R_{ij}$  as

$$\frac{\delta R_{ij}}{R_{ij}} = \sqrt{\left(\frac{\delta R_o}{R_o}\right)^2 + \left(\frac{\delta R_e}{R_e}\right)^2 + \left(\frac{\delta R_d}{R_d}\right)^2 + \left(\frac{\delta R_a}{R_a}\right)^2} . \quad (3.18)$$

### EoBO scenario

In EoBO conditions we deal with one more uncertainty related to the unknown occurrence time of the escaping moment in a situation not yet at equilibrium. When the gases are detected

 <b>Ricerca Sistema Elettrico</b>	<b>Sigla di identificazione</b>	<b>Rev.</b>	<b>Distrib.</b>	<b>Pag.</b>	<b>di</b>
	ADPFISS – LP2 – 051	0	L	16	25

is known the elapsed time  $T$  between detection and restart, but it's unknown the escaping moment that split the total time  $T$  in a first span in which the radioactive gases were building up and a second span in which they were decaying; since the growing and decaying constant are different the splitting cause an uncertainty on the initial tag gas ratio which must be accounted for.

We address  $T$  as the time between restart and detection and  $\tau$  the time between breaching and detection so that  $(T - \tau)$  is the irradiation time. With this nomenclature the activity at the detector becomes

$$A_i(\tau) = D\sigma_i\Phi N_{po\ i} e^{-\sigma\Phi_a(C+(T-\tau))} (1 - e^{-\lambda_i(T-\tau)}) e^{-\lambda_i\tau} \quad (3.19)$$

so that  $R_{ij}$  can be expressed in compact form as

$$R_{ij} = R_o R_e R_d R_a R_s \quad (3.20)$$

where the new term

$$R_s = \frac{1 - e^{-\lambda_i(T-\tau)}}{1 - e^{-\lambda_j(T-\tau)}} \text{ is the difference in the rate towards equilibrium of isotopes } i \text{ and } j.$$

The terms  $R_a$  and  $R_s$  are strongly interdependent and it's not easy to understand if it's a conservative assumption to take them separately, so they will be considered as one as  $R_t = R_a R_s$ . The detail treatment of this term is quite lengthy and involves a partial derivative of a bunch of exponentials, nothing difficult, but surely boring so only the final result will be stated

$$\frac{\delta R_t}{R_t} = A(\tau, T) \delta\tau, \quad (3.21)$$

where the amplification coefficient  $A(\tau, T)$  has its maximum value when the difference in  $\lambda$ s is high and when an high  $T$  and a low  $\tau$  are coupled.

The other factor are exactly the same as before (EoL) and can be combined statistically to give the final uncertainty which, from now on, will be labeled as  $U$ .

Coming back to the question of which minima to choose for the quanta; the creator of the methodology suggest to respect the EoBO quanta while preserving the EoL ratios because this is the most probable situation. Another choice would be to simply select the maximum quanta. What is best? Depends, of course, on the case at hand; usually the first option leads to much larger quanta than the other and if the volume in the pin is short that could create some problems. The advantage of the first option seems to be the possibility of not performing one exponential deconvolution if equilibrium conditions are reached at the rupture's time. Let's see if that's really the case.

From the detector the activity ratio  $R_{ij}$  is read; then the time between breaching and detection  $\tau$  is deconvoluted, being affected by some error (already discussed), ending up with

$$\frac{\sigma_i N_{po\ i} e^{-\sigma_i\Phi T} (1 - e^{-\lambda_i t})}{\sigma_j N_{po\ j} e^{-\sigma_j\Phi T} (1 - e^{-\lambda_j t})} \quad (3.22)$$

where the cross sections and decay constants are known, as well as  $T$  and  $t$  (there can be the splitting problem if not yet at equilibrium). The aforementioned advantage is to avoid the

 <b>Ricerca Sistema Elettrico</b>	<b>Sigla di identificazione</b>	<b>Rev.</b>	<b>Distrib.</b>	<b>Pag.</b>	<b>di</b>
	ADPFISS – LP2 – 051	0	L	17	25

deconvolution of the exponential in parenthesis which, however, is never an issue if we are at equilibrium since it can be performed exactly. So the choice of keeping the EoL ratios will not be pursued in the present work and the quanta will be the one able to respect both minimum detection sensibility requirements.

### 3.1.5. Fingerprints

Now that the quanta and the uncertainties have been fixed, it is possible to start with the creation of the various fingerprints in a number equal to the FAs in the core design at study. It will come in hand to define the so called uncertainty diameter  $d$  as

$$d = \frac{1 + U}{1 - U} \quad (3.23)$$

which represents the minimum distance that two ratios should have to overcome an uncertainty equal to  $U$ . So magnifying, in turn, the quanta of each isotope by  $d$  will create different fingerprints distinguishable from one another. In the end every fingerprints is made by combining different quantities of the selected gases. There's the clever possibility of graphically representing this concept using logarithms which transform multiplication in simple addition. Let's start by defining an integer  $n_i$  as

$$n_i = \log_d \left( \frac{\text{Actual quantity}_i}{q_i} \right), \quad (3.24)$$

where  $q_i$  is the quantum for gas  $i$ , so that the actual gas quantity can be expressed as

$$\text{Actual quantity}_i = q_i d^{n_i}. \quad (3.25)$$

Using this integer it is possible to represent every fingerprint with a four digit sequence (FS), for example FS = (0,0,0,0) means all gases loaded in quanta concentrations.

A tricky point must be made clear: we are interested in ratios, so FS = (0,0,0,0) and FS = (1,1,1,1) are identical for our purposes. One of the gases has always to be in its quanta amount (i.e. FS must have one digit always equal to zero) otherwise the FS in question will simply be a magnification of another FS with a lower overall gas quantity. This can be understood mathematically by taking the ratio of equation (3.25) for gas  $i$  and  $j$ , obtaining

$$\frac{\text{Actual quantity}_i}{\text{Actual quantity}_j} = \frac{q_i}{q_j} d^{n_i - n_j} \quad (3.26)$$

so that, if every digit of a FS is increased/decreased by the same amount the difference  $n_i - n_j$  will not change and the ratio will remain identical.

If we imagine every digit of a FS as a Cartesian co-ordinate in a 4-dimensional hyperspace, every FS will simply be a point. Since one digit is bound to be zero the points will lie in the four positive 3D volumes bounding 1/16 of the hyperspace.

The tag gas amount must be increased by  $d$ , that is: by 1 on the corresponding Cartesian axis, meaning that uncertainties can be represented as logarithmic spheres<sup>1</sup> of radius 1 around each

<sup>1</sup> These spheres will have a shorter radius in the positive direction ( $\log_d(1+U)$ ) and a longer one ( $\log_d(1-U)$ ) in the other.

FS point. The equivalence between FS = (0,0,0,0) and FS = (1,1,1,1) can also be understood graphically by noting that (just picture a 2D space for easiness) the line  $y = x$  is the “iso-ratio” line, so moving on that will not change the ratios of the FSs. In a general n-dimensional space the directions which represent iso-ratios are given by the cosine directors.

Summarizing until now, if a breaching occurs the daughter gases are detected and their activity measured, then starts a regression analysis to the initial concentration of the parent gases in the fresh pin. If the regression were error free the analysis would yield an exact 4-digit integer number identifying the faulted FA; due to the errors the result will be instead a quadruple of real numbers laying in the sphere surrounding the actual FS which indeed accounts for uncertainties.

The choice of the actual FS can be made e.g. by cost or volume optimization logics, depending of the priority of the designer; if the objective is indeed volume minimization, it's easy to understand that gases with the low quanta should be used more than the rest. The maximum quantity can be approximately calculated as

$$n_{\max,i} = \text{floor} \left( \frac{\log \left( \frac{q_j}{q_i} \right)}{\log d} \right), \quad (3.27)$$

where  $q_j > q_i$ . So the gases can be sort in quanta decreasing order and  $n_{\max,i}$  can be calculated for every gas relative to the one just before in the sorted list. This procedure defines limits for the co-ordinate axes and thus constrain the shape of the viable hyperspace. A simple example is reported in Table 3.2 where the total number of fingerprint is calculated accounting also for the 0 digit for every gas.

**Table 3.2: Example of volume optimization strategy**

Isotope	$n_{\max,i}$	1 <sup>st</sup>	2 <sup>nd</sup>	3 <sup>rd</sup>
Kr78	ref	0	0	1
Xe128	above+1	0	1	2
Xe126	above+2	2	3	4
Xe124	above+4	6	7	8
Number of FSs		21	64	206

### 3.1.6. Families

Until now the methodology were neglecting or oversimplifying some aspects in order to keep light on the founding principles, in this section we will release some of the limitations inherent in the method explain so far.

The flux is a good example; we not only have uncertainties about its value in a fixed point, but is quite different in the various regions of the core. If the spatial variation of the flux has to be taken into account by the elementary uncertainty  $\delta\Phi/\Phi$ , the uncertainty diameter  $d$  is bound to drastically increase, maybe effectively killing the possibility of practically implementing the methodology. A solution could be to divide the core in different zones, in

 <b>Ricerca Sistema Elettrico</b>	<b>Sigla di identificazione</b>	<b>Rev.</b>	<b>Distrib.</b>	<b>Pag.</b>	<b>di</b>
	ADPFISS – LP2 – 051	0	L	19	25

such a way to have, in each of them, the flux rather constant or at least ranging within a reasonable uncertainty. For being able to recognize the flux zones we can create families of fingerprints each one used in a different flux zones. For example using four gases it is possible to create 6 couples, 4 triplets and 1 quartet for a total of 11 families. Each family has its own uncertainties and characteristics which condition the number of combinations for a fixed maximum volume, and this must be kept in mind when coupling families and flux zones.

This way of working is very effective in covering the spatial flux gradient. For example, with 11 families and a flux uncertainty of 20% in each one it would be possible to cover a range from 1 to 0.086, more than a decade.

With this the methodology description is complete and various optimization options are left as degree of freedom to the designer that can choose his focal point, being that volume minimization, diameter reduction, flux covering, resolving power maximization and so on.

### ***3.2.Application to the ALFRED design***

The methodology explained at length in the previous section will now be applied to the ALFRED core design with the following objectives:

- minimizing the loaded volume in the pins and
- maximizing the resolving power.

Objectives can be seen as guidelines that help us moving in the design hyperspace, but what is really important are constrains which, usually, strongly limit the viable space where the solution can live. For the ALFRED case the following constrains must be kept in mind:

- the volume available in the pin is  $600 \text{ Ncm}^3$  and, given the necessity to contain cladding stresses due to fission product build up in the plenum, the amount of tag gas cannot exceed  $2\div 3\%$  of the total volume, so in the end,  $V_{\max} = 15 \text{ Ncm}^3$ .
- An activation study [5] revealed that at equilibrium the activity of the isotope Xe129m, daughter of Xe128, in the core is around  $2.2 \cdot 10^{12} \text{ Bq}$  which means around  $10^8 \text{ Bq}$  in one pin. The equilibrium activity of the loaded Xe129m must thus be much greater than this value or better avoid the use of this tag gas.
- The sensibility of the detector,  $S$ , is set to  $10 \text{ Bq}$ .

The next step is to calculate the quanta both in EoL and EoBO, for the purpose, the assumed values of the parameters of interested are listed in Table 3.3 where  $f$  is the load factor which scales the actual depletion time. The flux uncertainty is variable because it depends on the family distribution as we shall see.

**Table 3.3: Values of the parameters of interest assumed in the analysis**

Parameter	Value		unit
	EoL	EoBO	
$\Phi$	$10^{15}$	$10^{15}$	n/cm <sup>2</sup> s
$T$	5	5	y
$\tau$	0.5	0.5	h
$D$	$10^{-5}$	$10^{-5}$	–
$\Phi_a$		$10^{14}$	n/cm <sup>2</sup> s
$C$		4	y
$T_{BO}$		1	d
$f$	0.85	0.85	–
$\frac{\delta\sigma}{\sigma}$	10	10	%
$\frac{\delta\Phi}{\Phi}$	Variable	Variable	–
$\delta\tau$	0.5	0.5	h

The quanta resulting are reported in Table 3.4.

**Table 3.4: Quanta identified for the limiting scenarios**

Isotope	Quanta [Ncm <sup>3</sup> ]	
	EoL	EoBO
Kr78	$5.88 \cdot 10^{-3}$	0.155
Xe124	$2.0 \cdot 10^{-5}$	$3.0 \cdot 10^{-4}$
Xe126	$7.5 \cdot 10^{-4}$	0.4

As explained in section 3.1.4 the quanta are selected as the maximum of the two scenario, in this case restart is always the most thighting situation and as such its quanta are taken as reference.

Focus has been given to a strategy which avoided utilizing the tag gas Xe128 in order to overcome the strong background noise due to the fission products presence. That left us with only 3 tag gases for a total of 4 families.

With the assumed elementary uncertainties and a flux uncertainty taken at 40% (as we shall see this is the limiting flux variation) the error propagation results are summarized in Table 3.5 where is easy seen that for uncertainties EoL is the most penalizing condition. The dominant uncertainty is the one on  $R_d$  due to the relative high depletion of Xe124.

**Table 3.5: Tag gas uncertainties analysis for ALFRED triplet family**

Parameter	Uncertainty	
	EoL	EoBO
$\frac{\delta R_o}{R_o}$	0.05	0.05
$\frac{\delta R_e}{R_e}$	0.15	0.15
$\frac{\delta R_d}{R_d}$	0.27	0.13
$\frac{\delta R_a}{R_a}$	0.02	
$\frac{\delta R_t}{R_t}$		0.01
$U$	0.31	0.2

A similar analysis has been performed for every family having care of using the pertinent cross sections and decay constants which leads to quite different uncertainty diameters and thus capabilities of hosting combinations in steep flux gradient situations.

The number of combinations possible with each family under the constrain of maximum volume less than 15 Ncm<sup>3</sup> and different flux gradients are reported in Table 3.6, where the method used to calculate them was explained in subsection 3.1.5.

**Table 3.6: Possible combinations for every family under different flux gradients**

$\frac{\delta\phi}{\phi}$	20%	30%	40%
Kr78 – Xe126	23	23	23
Kr78 – Xe124	34	28	24
Xe124 – Xe126	32	26	22
Kr78 – Xe124 – Xe124	430	300	220

The choice was to divide the core in 3 flux zones ( $\frac{\delta\phi}{\phi} = 40\%$  in each zone) and assign to one flux zones 2 families based on the results obtained with the deterministic code ERANOS [8]. The flux is pretty flat in the inner region and then, in the last two rings of FAs drops steeply (Figure 3.1), for this, 1 flux zone was assigned to each one of the last two outer ring and the others inner FAs were gathered in the last flux zone. Because this last zone has 111 assemblies the triplet family was assigned to it, the last ring has only 18 FAs so the couple Kr78 – Xe126 (pretty insensitive to flux uncertainties due to the low parent depletion) was used and finally the remaining 42 assembly were filled with the other couples Kr78 – Xe124 and Xe124 – Xe126. The layout just described along with the FSs used are plotted in Figure 3.2, where the FS distribution was chosen in order to minimize the volume loaded.

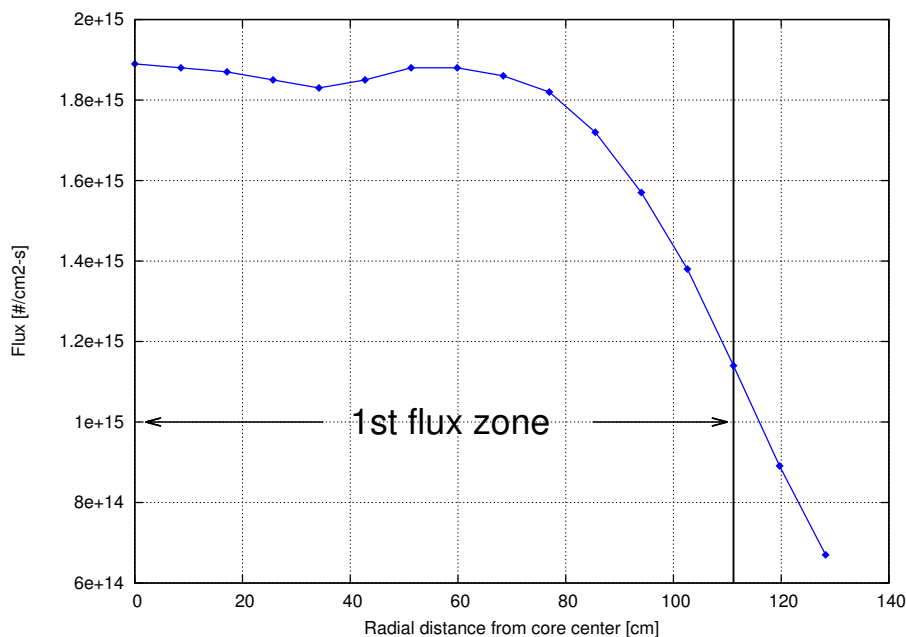


Figure 3.1 - Flux traverse from core center to the periphery, passing through a safety rod.

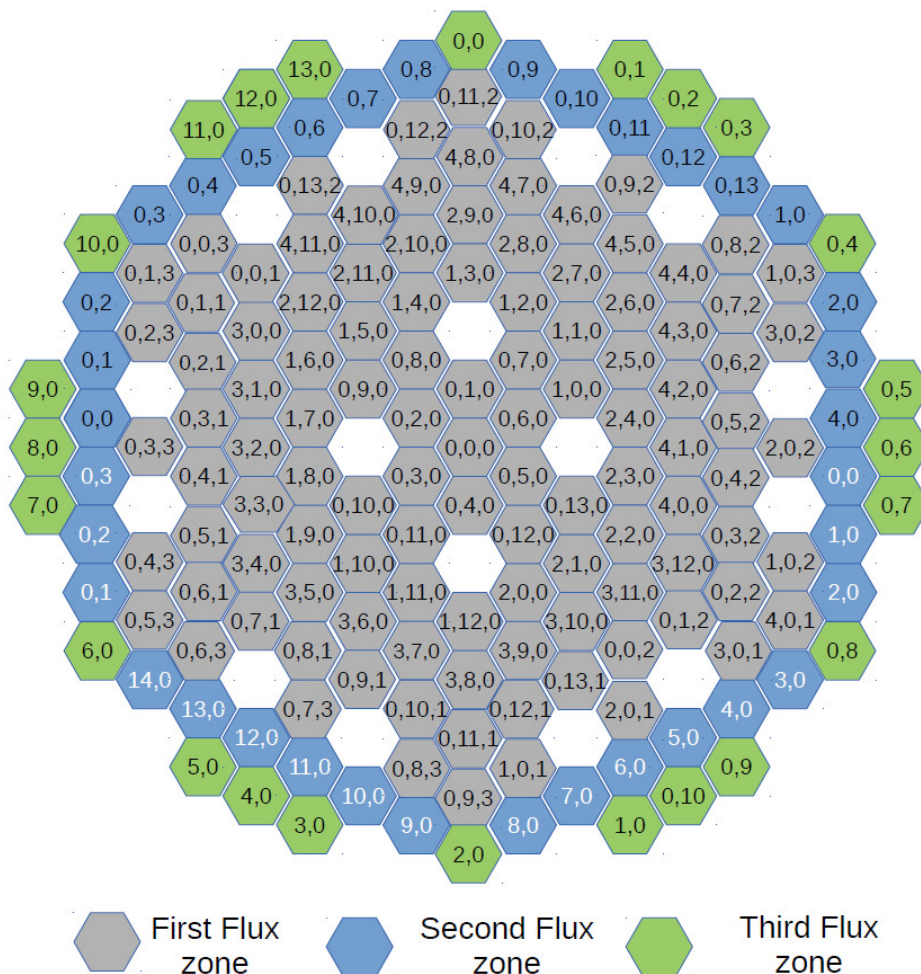


Figure 3.2 - Tag layout over the ALFRED core. The isotope family order is: Kr78 – Xe124 – Xe126, Kr78 – Xe126, Kr78 – Xe124 and Xe124 – Xe126 (white).

As an example the fingerprints' combinations composing the triplet family is reported in Figure 3.3 with the graphical representation described in subsection 3.1.5.

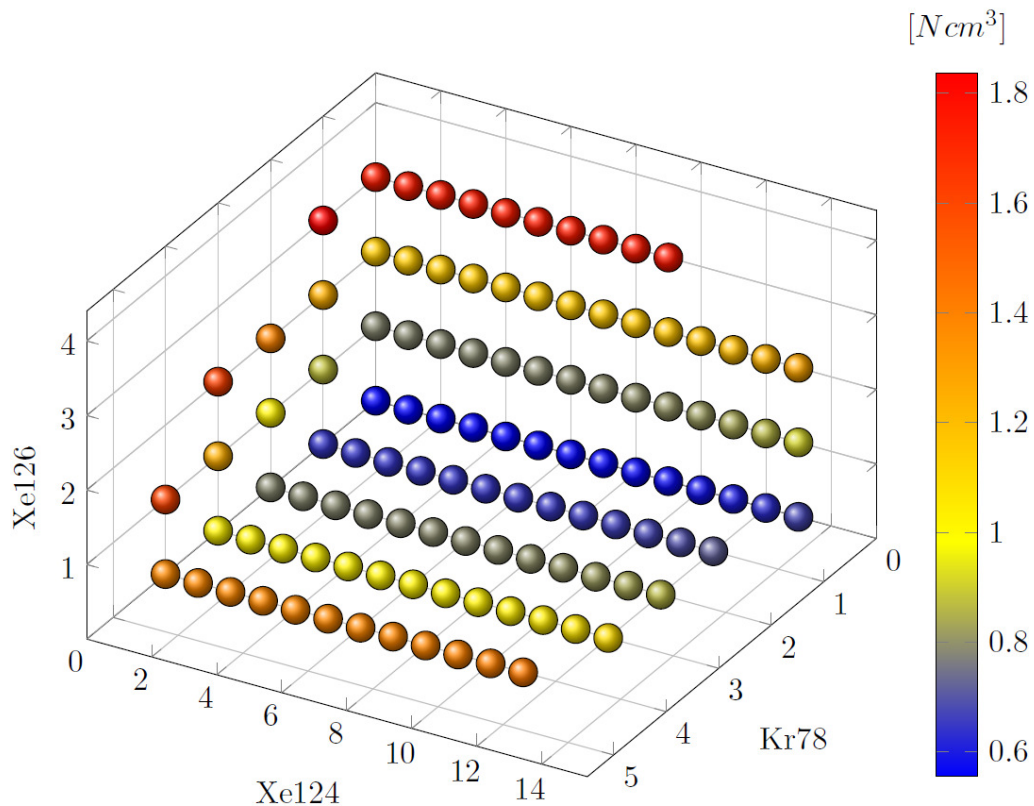


Figure 3.3 - Flux traverse from core center to the periphery, passing through a safety rod.

The other family FS are summarized in Table 3.7 where the maximum extension of each axes of the FSs is reported for each isotope. Finally the maximum volume loaded in each flux zone is reported in Table 3.8: as can be seen, the 15 Ncm<sup>3</sup> constrain has been largely fulfilled and the higher values are mostly at the border where clad stresses are less of a concern.

Table 3.7: Maximum extension of FP axes along each isotope direction

	Maximum extension
Kr78 – Xe126	(13,10)
Kr78 – Xe124	(4,13)
Xe124 – Xe126	(14,3)

Table 3.8: Maximum volume of tag gases for each flux region

	Maximum volume [Ncm <sup>3</sup> ]
Region 1	3.06
Region 2	2.72
Region 3	10.3

 <b>Ricerca Sistema Elettrico</b>	<b>Sigla di identificazione</b>	<b>Rev.</b>	<b>Distrib.</b>	<b>Pag.</b>	<b>di</b>
	ADPFISS – LP2 – 051	0	L	24	25

#### 4. Conclusions

Two studies have been presented in this report, both regarding a preliminary approach into ALFRED core monitoring.

The first study focused on the investigation of the viability of a neutron detection system (here called Operation Monitoring and Protection Detection system, OMPD) to be inserted into the reactor vessel and close to the core (in-vessel ex-core) for the continuous monitoring of the spatial flux distribution and a redundant control on the flux level (the first monitoring being duty of the standard Full-Range Flux Detection system, FRFD, operating ex-vessel).

Following a review of the instrumentation commercially available, the simulation of the detector response in positions suitably reserved in the outlet section of the fuel elements has been performed by means of MCNP6.

The results here presented seem to indicate the viability of this option, and a good resolving power in detecting changes to the spatial flux distribution due to any possible initiating event (the spurious inadvertent withdrawal of one Control Rod was used as example, being one of the initiators raising most concerns).

The second study focused on the adaption of a simple yet sound and reliable methodology for discriminating the unique tags of different “cocktails” of gas mixtures to be added to the pins of each fuel assembly so as to individuate the location of possible cladding breaches.

When tuned to the ALFRED spectrum and fission products – for the selection of the most appropriate tag gases – the proposed methodology fully satisfies the availability of a number of “cocktails” without immobilizing sensitive volumes in the plenum of the pins, and still ensuring various optimization options as degrees of freedom to the designer, who can choose his focal point, being that volume minimization, diameter reduction, flux covering, resolving power maximization and so on.

Sufficient unique mixtures have been found by making use of three out of the four gases initially proposed, notably: avoiding the use of Xe128, still largely respecting the limit on the maximum preloading volume. The elimination of Xe128 among the tag gases simplifies the procedure, since its daughter – Xe129m – is also produced as a gaseous fission product within the pins, so the use of its father might have affected the detected signal to be identified.

 <b>Ricerca Sistema Elettrico</b>	<b>Sigla di identificazione</b>	<b>Rev.</b>	<b>Distrib.</b>	<b>Pag.</b>	<b>di</b>
	ADPFISS – LP2 – 051	0	L	25	25

## References

- [1] EURATOM Seventh Framework Programme. Lead-cooled European Advanced DEMonstration Reactor (LEADER). Proposal/Contract no. FP7 – 249668, (2010), <http://www.leader-fp7.eu/default.aspx>.
- [2] G. Grasso *et al.* Ottimizzazione del progetto di nocciolo di ALFRED. Technical report ADPFISS-LP2-050, ENEA, September 2014.
- [3] PHOTONIS. Neutron and Gamma Detectors. Technical brochure.
- [4] NEA Data Bank. Validation of the JEFF-3.1 Nuclear Data Library. JEFF report 23, OECD-NEA, February 2013.
- [5] C. Petrovich *et al.* Definition of the ALFRED core and neutronic characterization. Technical Report LEADER-DEL007-2012 rev. 1, March 2013.
- [6] J.T. Goorley. MCNP6.1.1-Beta Release Notes. Technical report LA-UR-14-24680, Los Alamos National Laboratories, 2014.
- [7] F. Padoani, C. Artioli and G. Glinatsis. Performance and Characteristics of a Small-Sized Oxide-Fuelled Fast Reactor (PRISM) for the burning of excess plutonium. In *Science for Peace*, vol. 1, pages 163-198, UNESCO, 1996.
- [8] G. Rimpault *et al.* The ERANOS Code and Data System for Fast Reactor Neutronic Analyses. In Proc. *International Conference on the New Frontiers of Nuclear Technology: reactor physics, safety and high-performance computing (PHYSOR 2002)*, Seoul, Korea, October 7-10, 2002.